Thermally tunable phonon–plasmon polariton modes at hexagonal boron nitride (hBN) and indium antimonide (InSb) interfaces

Journal of Optics

PAPER • **OPEN ACCESS**

Thermally tunable phonon–plasmon polariton modes at hexagonal boron nitride (hBN) and indium antimonide (InSb) interfaces

To cite this article: Tahseen Sana *et al* 2024 *J. Opt.* **26** 115006

OPEN ACCESS
IOP Publishing
Journal of Optics
J. Opt. **26** (2024) 115006 (11pp)
https://doi.org/10.1088/2040-8986/ad8459

Thermally tunable phonon–plasmon polariton modes at hexagonal boron nitride (hBN) and indium antimonide (InSb) interfaces

Tahseen Sana[1], Majeed A S Alkanhal[2], Ahtisham Ali[3], Hafeez Ullah[1], Abdul Ghaffar[4], Yasin Khan[2] and Muhammad Zeshan Yaqoob[5,*]

[1] Biophotonics Imaging Techniques Laboratory, Institute of Physics, The Islamia University of Bahawalpur, Bahawalpur, Pakistan
[2] Department of Electrical Engineering, King Saud University, Riyadh, Saudi Arabia
[3] Dipartimento di Elettronica e Telecomunicazioni, Politecnico di Torino, Torino, Italy
[4] Department of Physics, University of Agriculture, Faisalabad, Pakistan
[5] Department of Physics, Government College University, 38000 Faisalabad, Pakistan

E-mail: zeeshaan32@yahoo.com

Received 31 July 2024, revised 26 September 2024
Accepted for publication 8 October 2024
Published 17 October 2024

Abstract

This work examines the propagation of thermally tunable phonon–plasmon modes at the interfaces of hexagonal boron nitride (hBN) and isotropic indium antimonide (InSb). Both theoretical modeling and numerical simulations are carried out to analyze the effect of temperature on surface wave behavior. hBN is realized as a polar material via the Lorentzian model, while InSb is modeled as a temperature-sensitive material (TSM) in the framework of Drude's model. The possible plasmon–phonon polaritonic interactions are studied for the TSM–elliptic type interface and TSM–hyperbolic type interface. It is reported that by varying the temperature, the surface modes can be tuned for the lower and upper Reststrahlen (RS) bands of hBN. The dispersion curve, effective mode index, propagation length, and phase speed are computed for each case under different temperatures. It is concluded that the hBN–InSb-based phonon–plasmon polariton modes are actively tuned by changing the external temperature in the lower and upper RS bands. Surface waves propagating across the interface can be modulated from the terahertz (THz) region to the infrared (IR) region by changing the temperature of InSb. This study will help researchers to design innovative thermo-optical sensors, plasmonic platforms, detectors, and surface waveguides in the THz and IR regions.

Keywords: phonon, plasmon, polariton, hexagonal boron nitride, surface waves, infrared/terahertz, thermo-optical materials

* Author to whom any correspondence should be addressed.

1. Introduction

The exploration of electromagnetic (EM) waves as they propagate through materials' surfaces has drawn the interest of the scientific community due to its potential applications (i.e. signal processing [1], surface communication [2], modulators [3], chemical sensing [4], tissue detection [5], plasmonic solar cells [6], spectroscopy [7], near-field imaging [8], surface enhanced Raman scattering [9], and biosensing [10]). To minimize the major challenges in the design of innovative device architectures and real-world platforms, we must understand and control these waves propagating at the interfaces between diverse materials [11]. EM waves that decay away from the interface perpendicularly and propagate along the interface between two optically different media show a significant role in several areas of science and technology, including microscopy and technological applications [12, 13]. EM surface (EMS) waves are useful for optical devices like waveguides, sensors, and filters because they provide light confinement as well as effective transmission of low-loss information over shorter distances [14]. Different types of interfaces support various kinds of waves, like chiral surface waves, nonlinear surface waves, Dyakonov surface waves (DSWs), and surface plasmon polariton (SPP) waves. Nonlinear surface waves propagate at nonlinear interfaces, DSWs propagate along isotropic–anisotropic interfaces, and SPP waves propagate along metal–dielectric interfaces [15]. In the 20th century, Dyakonov suggested the existence of a unique type of surface wave at the interface between two transparent dielectric materials, wherein at least one of the materials is anisotropic uniaxial in nature [16]. DSWs are regarded as lossless surface waves because their partnered materials are lossless dielectrics [17]. DSWs have been explored theoretically in a variety of anisotropic media, including hyperbolic metamaterials [18], biaxial crystals [19], chiral material [20], magnetic materials [21], and nonhomogeneous media [22]. Several scientists have proposed various strategies, such as using metasurfaces and nanocomposites, to manipulate EM waves across diverse spectral ranges. The multiple plasmonic structures for the visible range have been investigated for their potent connections with biomolecules and nanostructures, as well as their possible use in waveguides, biosensing, drug delivery, and nano-photonics [23].

Recently, Hexagonal boron nitride (hBN) has garnered significant attention in the fields of optics and photonics, primarily due to its remarkable characteristics, such as a wide bandgap, high thermal conductivity, and robust mechanical properties [24]. Due to the weak nature of Van der Waals forces [25], hBN shows extreme anisotropy, which is why it is used as a promising anisotropic material to study the propagation of DSWs [26]. Merano carried out the theoretical computations to study the spatially confined surface modes on the single layer of hBN and verified the existence of TE polarized surface modes supported by the hBN layer in visible spectrum [27]. Zhu *et al*, carried out a detailed theoretical investigation regarding the possible solution of the propagating DSWs at the hBN-isotropic dielectric material. The propagation characteristics of DSWs (angular existence domain, effective index, propagation length and field profiles) have been investigated under two types of interfaces i.e. dielectric-elliptic and dielectric-hyperbolic [28]. Its two-dimensional nature facilitates seamless integration with other 2D materials, like graphene and transition metal dichalcogenides, which is advantageous for the creation of innovative optoelectronic devices [29–31]. Recent research highlights the role of h-BN as an effective substrate for quantum emitters, significantly improving their optical characteristics and longevity [32]. Furthermore, the unique phonon interactions in h-BN make it an ideal candidate for advancing thermo-optical devices for communication and sensing [30, 33]. Its substantial exciton binding energy also positions h-BN as a key player in ultrafast photonic applications, offering pathways for the development of advanced photonic circuits and light-emitting technologies. These developments illustrate the promising potential of h-BN in shaping the future of optical technologies such as biosensor devices, optical detectors, and surfaces of thin-film solar cells [34, 35].

In addition, the temperature plays an important role in designing low-loss optical waveguides and optical devices. The characteristics of the temperature-sensitive materials (TSMs) can be altered by varying the external temperature, and these temperature-dependent materials possess electronic, phase, optical, and structural properties [36]. Since TSMs have restricted gaps, they are sensitive to very minimal temperature changes, which can drastically modify their thermal properties to support surface waves. Furthermore, the frequency range of TSMs is influenced by the semiconductor's plasma frequency. Unlike metals and dielectrics, the semiconductor's frequency is highly sensitive to temperature and is determined by the concentration of free carriers. A few semiconductors, like indium antimonide (InSb), can be used in metal–dielectric materials in place of metals because they have an appropriate carrier density to allow their frequency to be positioned in the terahertz (THz) range [37]. Recently the tunable surface wave propagation supported by the InSb have been reported by many researchers i.e. Macaky and Lakhtakia proposed the temperature sensitive hyperbolic composite structure based upon the InSb and investigated the propagation of the surface waves along the interface of hyperbolic structure and isotropic material. They reported that the characteristics of the propagating surface waves can be tailored by the temperature variation and composition fill factor [38]. Further, the Moradi discussed the theoretical findings on the thermally tunable DSWs supported by the engineered metamaterial structure based upon the InSb nanowires. It has been reported that for the low temperature, the indium antimonide behave as dielectric material supports the DSWs while for the high temperature the InSb behave as conductor, supports the DSPWs [39]. Yaqoob *et al*, carried out the theoretical investigation on the temperature dependent characteristics of surface waves/SPP waves propagating along the graphene-InSb interface. It has been reported that the graphene parameters and InSb both can be

used to manipulate the characteristic of surface waves, further it is concluded that the use of graphene layer on the substrate of the InSb significantly improve the tunability control on the surface waves [40]. Recently, Sana *et al*, studied the hybrid DSWs propagation along the interface of uniaxial metamaterial-InSb and concluded that the apart from the thermal tunability, the interface supports the two distinct surface waves i.e. pure DSWs for $T \in [200, 240]$ K and hybrid SPP waves for $T \in [290, 360]$ K [41]. Keeping in view of these developments, this research paper investigates the hBN-based planar structure for EMS wave propagation. The primary objective is to analyze the surface wave propagation along the interfaces between TSMs like InSb and hBN, and the main task is to study the existence of DSWs along the interfaces of hBN and InSb. InSb is an appropriate material having a smaller bandgap for changing the propagation of surface waves due to its attractive optical and electrical features with significant temperature dependence [42]. By perceiving and broadening the interactions between the interfaces of InSb–hBN and EM waves, it is possible to produce new devices with useful applications in photonics and optoelectronics. The interactions between plasmon and phonon polaritons are examined for both the TSM–elliptic and TSM–hyperbolic type interfaces. The findings indicate that adjusting the temperature allows for the tuning of surface modes within the lower and upper Reststrahlen (RS) bands of hBN. We also compute the characteristics of surface waves, such as dispersion length, effective mode index, propagation length, and phase speed, and analyze the influence of temperature on these characteristics. We find that the properties of surface waves can be adjusted by varying the temperature. The calculated results can be applied to the planning of chemical sensing and thermo-optical waveguides as well as communication modules.

2. Analytical formulation/modeling of problem

In this geometry, the hBN-based structure, which supports the propagation of EMS waves, is observed. This planar structure manifests as anisotropic substrates or platforms. To realize the proposed structure, the different synthesis and deposition techniques can be used as reported in [43, 44]. The primary goal of the proposed effort is to examine how surface waves propagate over the interfaces between hBN and TSMs like InSb, as shown in the below figure 1.

Consider the propagation of a monochromatic DSW along the z-axis characterized by a wave vector $\gamma = (0, 0, \gamma)$. The DSW can be initiated only by the superposition of the transverse-electric (TE) and transverse-magnetic (TM) waves whose wave vectors have a z-axis component identical to q and cannot be initiated either by the pure TE or TM wave. This polarization hybridization [16] contains four evanescent independent solutions: two of the solutions are due to a dielectric medium having diverse polarizations with complex-valued TE and TM modes, and the other two solutions are due to a uniaxial medium having ordinary and extraordinary modes. We

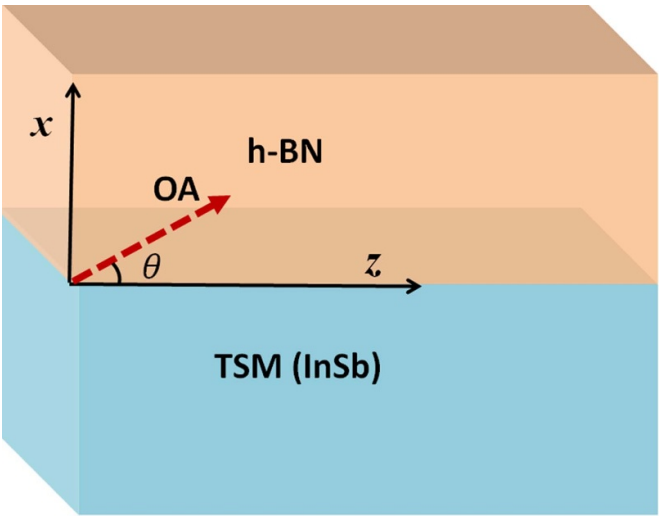

Figure 1. EMS wave propagation along hBN–InSb interface.

consider that the interface coincides at the $x = 0$ plane. The isotropic medium is engaged in the half-space $x > 0$, while the other half-space $x < 0$ is occupied by the crystal whose optic axis is parallel to the described interface. This optic axis is supposed to be the z-axis and form an angle 'θ' with the surface wave's phase velocity. We have two independent field modes in the isotropic medium having unlike polarizations and the same wave vector $\gamma_1 = (ik_1, \gamma_1 0, \gamma)$, where k_1 is illustrated as

$$\gamma^2 - {k_1}^2 = \varepsilon_{T.}. \tag{1}$$

The other two independent field modes (i.e. extraordinary and ordinary modes) of the uniaxial medium have the wave vectors $\gamma_2 = (-ik_2, 0, \gamma)$ and $\gamma_3 = (-ik_3, 0, \gamma)$, respectively, and are controlled by the following dispersion relations:

$$\frac{\gamma^2 \sin^2\theta - k_2^2}{\varepsilon_{||}} + \frac{\gamma^2 \cos^2\theta}{\varepsilon_{\perp}} = 1 \tag{2}$$

$$\gamma^2 - k_3^2 = \varepsilon_{\perp}. \tag{3}$$

Maxwell equations (i.e. $[\gamma E] = H$ and $[\gamma H] = -\varepsilon E$) show the resulting solutions in the region $x < 0$.

For an extraordinary wave, we have

$$\begin{aligned} E &= \left(ik_2\gamma\cos\theta, -\varepsilon_{\perp}\sin\theta, \left(\varepsilon_{\perp} - \gamma^2\right)\cos\theta\right) \\ H &= \left(\gamma\varepsilon_{\perp}\sin\theta, ik_2\varepsilon_{\perp}\cos\theta, ik_2\varepsilon_{\perp}\sin\theta\right). \end{aligned} \tag{4}$$

For an ordinary wave, we have

$$\begin{aligned} \mathrm{E} &= (\gamma\sin\theta,\ ik_3\cos\theta,\ ik_3\sin\theta) \\ H &= \left(-i\gamma k_3\cos\theta, \varepsilon_{\perp}\sin\theta, {k_3}^2\cos\theta\right). \end{aligned} \tag{5}$$

To show the TE and TM waves in the region of the half-space $x > 0$, the following independent solutions are deduced:

for TE, we have

$$E = (0, 1, 0)$$
$$H = (-\gamma, 0, \mathrm{i}k_1)\,. \tag{6}$$

For TM, we have

$$H = (0, \varepsilon_T, 0)$$
$$\mathrm{E} = (\gamma,\ 0,\ \mathrm{i}k_1)\,. \tag{7}$$

All of the above-mentioned wave vectors are related in terms of $^{\omega}/_{c}$, where c and ω stand for speed of light and wave frequency, respectively. For regions $x < 0$ and $x > 0$, we will get solutions by linearly combined equations (4) & (5) and (6) & (7) respectively. We anticipate that the tangential components of fields E and H will be continuous at the interface. This yields the mathematical equation

$$k_3\,(k_1 + k_3)\left(\varepsilon_\perp k_1 k_2 + \varepsilon_T {k_3}^2\right)\cos^2\theta = \varepsilon_\perp\,(k_1 + k_2)\,(\varepsilon_\perp k_1 + \varepsilon_T k_3)\sin^2\theta. \tag{8}$$

If the angle θ is known, a set of equations (1)–(3) and (8) provides four unknowns: k_1, k_2, k_3, and γ. After algebraic operations, we are able to simplify equation (8) to a more practicable form via equations (1)–(3) [16]

$$(k_1 + k_2)\,(k_1 + k_3)\,(\varepsilon_T k_3 + \varepsilon_\perp k_2) + (\varepsilon_\parallel - \varepsilon_T)\,(\varepsilon_\perp - \varepsilon_T)\,k_3 = 0. \tag{9}$$

The solution of the above computed equation led to existence of DSWs at the hBN-InSb interface. To get the insight of the analytical solution, the numerical results have been computed in the results and discussion of this manuscript to estimate the plasmon and phonon polaritons for both the TSM–elliptic and TSM–hyperbolic type interfaces.

3. Results and discussion

In this section, the numerical results have been described in two categories, in the first part the EM modeling of the hBN and InSb has been presented while in the remaining subsections the surface polaritonic and plasmonics interactions at different ranges of temperature and frequency have been investigated for the hBN-InSb interfaces. All the kernels and simulations have been computed in the Mathematica software pack.

3.1. Permittivity graph for hBN

The permittivity of the hBN (polar dielectric) axis can be illustrated by a single Lorentzian function [25]

$$\varepsilon_m(\omega) = \varepsilon_{\infty,m} + \varepsilon_{\infty,m}\frac{(\omega_{\mathrm{LO},m})^2 - (\omega_{\mathrm{TO},m})^2}{(\omega_{\mathrm{TO},m})^2 - \omega^2 - (j\omega\Gamma_m)}. \tag{10}$$

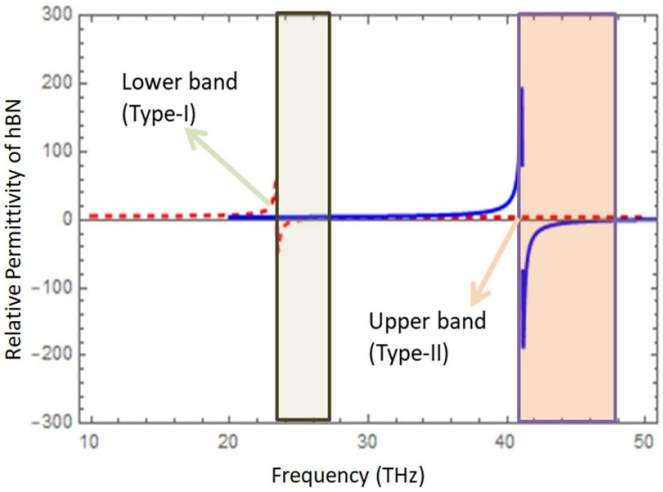

Figure 2. Upper and lower RS bands of hBN permittivity in relation to THz frequency.

In the above expression, ω_{LO} and ω_{TO} are related to the longitudinal and transverse optical phonon frequencies, respectively. Here, $m = \parallel$ or$\perp$ is associated with the transverse or z-axis, respectively. Moreover, each optical frequency possesses two values in the lower and upper RS bands (i.e. $\omega_{\mathrm{TO},\perp} = 41.1$ THz, $\omega_{\mathrm{LO},\perp} = 48.3$ THz, $\omega_{\mathrm{TO},||} = 23.4$ THz, $\omega_{\mathrm{LO},||} = 24.9$ THz), and ε_m is the high-frequency permittivity having values $\varepsilon_{\infty,\perp} = 4.87$ and $\varepsilon_{\infty,||} = 2.95$. In addition, Γ_m is related to the damping factor having values $\Gamma_\perp = 0.15$ THz and $\Gamma_\parallel = 0.12$ THz. The real part of the permittivity of hBN is displayed in figure 2. The upper and lower RS bands are two modes that are associated with the Type-I and Type-II hyperbolicity of hBN, as can be seen in this image. These frequency ranges are displayed in figure 2 as brown and purple rectangles, respectively. It is commonly known that hBN supports two separate RS bands. The higher (41.1 THz $< \omega <$ 48.3 THz) and lower (23.4 THz $< \omega <$ 24.9 THz) RS bands show the hyperbolicity of Type-I and Type-II [28].

3.2. Modeling of InSb

The ability of semiconductors to control permittivity by adjusting the carrier density is the basis for their application to tunable TSMs. InSb, a well-known semiconductor, is a great choice for a thermally adjustable material. Because of its unique characteristics, which include its small band gap, strong electron mobility, low effective mass, and extremely temperature-dependent carrier density, slight variations in temperature can readily affect the material's permittivity. The Drude model yields the complex-valued relative permittivity of InSb in the THz frequencies [39, 41]

$$\varepsilon_{\mathrm{InSb}} = \varepsilon_\infty - \frac{\omega_p^2}{\omega^2 + \mathrm{i}\gamma\omega}, \tag{11}$$

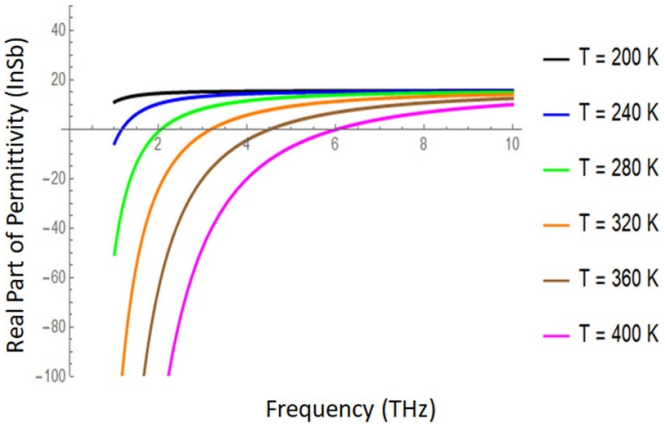

Figure 3. Effect of temperature on real part of InSb permittivity as function of THz frequency.

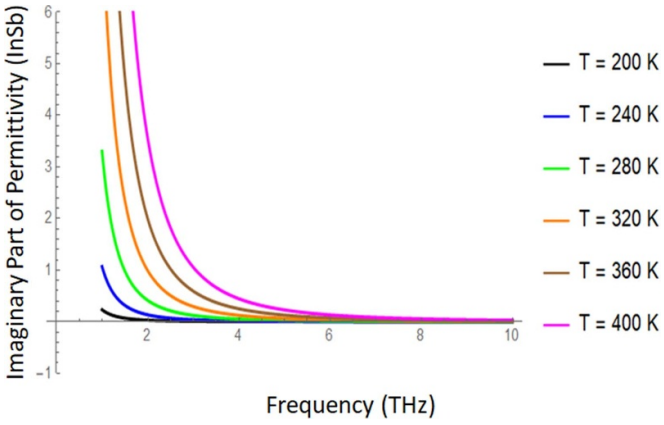

Figure 4. Impact of temperature on imaginary part of InSb permittivity as function of THz frequency.

where ω_p and ε_∞ indicate the plasma frequency and high-frequency range of relative permittivity, respectively. The damping constant is shown here by γ. The plasma frequency can be calculated as

$$\omega_p = \sqrt{\frac{Nq_e}{0.015\ \varepsilon_o m_e}}. \tag{12}$$

The intrinsic density of the charge carrier, the charge on the electron, and the electronic mass all influence the plasma frequency. Here, the electronic mass and charge on the electron are 9.1×10^{-31} kg and 1.6×10^{-19}C, respectively, and $\gamma is\ \pi \times 10^{11}$ rad s^{-1}. The Boltzmann constant, temperature, and bandgap significantly affect the intrinsic carrier density (N). It is computed as $= 5.76 \times 10^{20}\ T^{3/2} \exp(-\frac{E_g}{2k_B T})$. The values of E_g and k_B are 0.26 eV and 8.62×10^{-5}eV K^{-1}, respectively. We can state that the plasma frequency is affected by temperature in the same way that the intrinsic carrier density (N) depends on temperature (T). Thus, it is possible to modify the plasma frequency by varying InSb's temperature. Hence, variations in temperature parameters can impact InSb's relative permittivity [40].

Figure 3 displays a graphic representation of the effect of temperature on InSb's actual permittivity according to frequency. Here, the temperatures examined are $T = 200$ K, 240 K, 280 K, 320 K, 360 K, and 400 K. As the temperature rises, the permittivity of InSb vs. frequency gradually decreases.

The influence of temperature on the imaginary component of InSb permittivity is graphically depicted in figure 4 at the temperatures $T = 200$ K, 240 K, 280 K, 320 K, 360 K, and 400 K. Figure 4 illustrates how InSb's permittivity rises as the temperature rises, since the intrinsic carrier density (N), which can be adjusted by changing the temperature in accordance with equations (6) and (7), determines the plasma frequency of InSb. The figure indicates that an increase in temperature results in a rise in InSb's plasma frequency. It is clear from figure 3 how much the permittivity of InSb is affected by the plasma frequency and the surrounding temperature. The real and imaginary components of permittivity of the InSb can be adjusted by altering the external temperature, as shown in figures 3 and 4. At a frequency range of 10 THz, the temperature rises from 200 to 400 K, and figure 3 clearly illustrates the shift in the real part of permittivity from positive to negative values. However, for frequencies higher than 10 THz, the effect of temperature on Re(ε_{InSb}) becomes insignificant. On the other hand, as temperatures increase up to a frequency range of 8 THz, the imaginary part of permittivity increases, as shown in figure 4. It can be observed that the permittivity of InSb exhibits insulator behavior at $T = 200$ K and metal behavior at $T > 200$ K. Furthermore, only when the actual permittivity values of the adjacent materials are opposite in sign are surface waves supported at their interface [40]. In this way, ε_{InSb} can be adjusted by changing the temperature and set to the desired spectral range.

3.3. *Surface waves at TSM–elliptic interface (Type-1)*

Type-I hBN is linked to the lower RS band. The lower THz frequency range, or 23.4 THz $< \omega <$ 24.9 THz, is represented by the lower RS band. The permittivity range for Type-I is $\varepsilon\| < 0$ and $\varepsilon\perp > 0$. For Type-I, the results of numerical calculations are shown while accounting for the propagation length, phase velocity, effective mode index, and dispersion relation.

3.3.1. Dispersion curve analysis. Here, the results of numerical computations are displayed for DSW propagation in the THz frequencies at the interface between InSb and an anisotropic dielectric material, taking into consideration the dispersion relation in equation (9). The dispersion curves of DSWs are shown in figure 5 by considering nine different temperatures. The anisotropic dielectric, TSM substrate, and dispersion relation (equation (10)) were numerically solved in order to produce the dispersion curves.

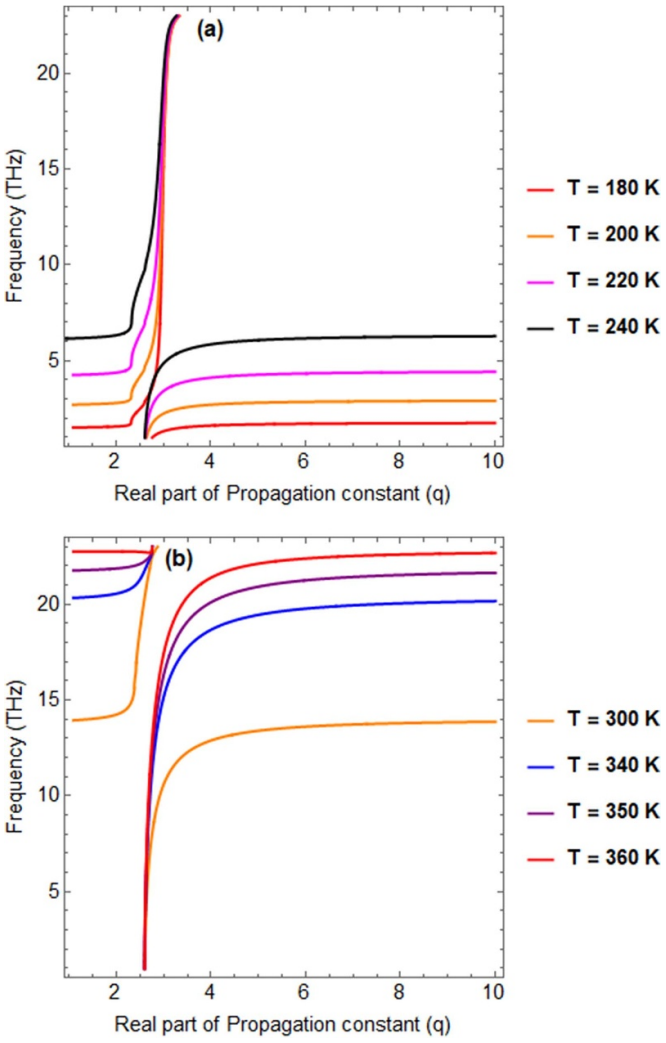

Figure 5. Dispersion curves for Type-I surface waves under temperature variation supported by hBN–InSb interface. (a) $T \in [180,\ 240]$ K (b) $T \in [300,\ 360]$ K.

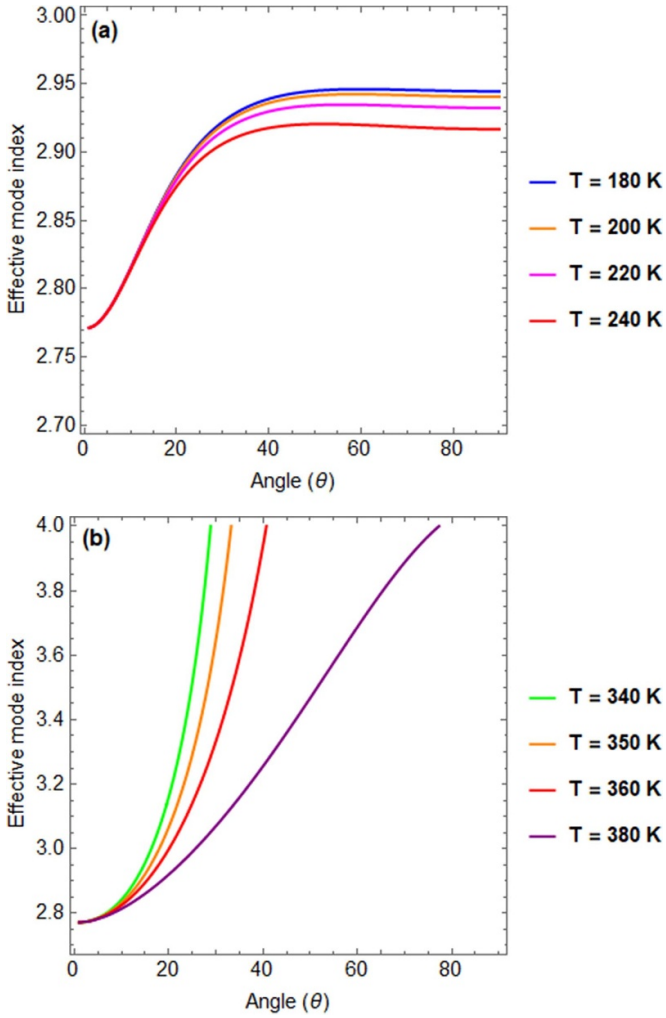

Figure 6. Effect of temperature on effective mode index (N_{eff}) at 23.9 THz supported by hBN–InSb interface for Type-I surface wave propagation. (a) $T \in [180,\ 240]$ K (b) $T \in [340,\ 380]$ K.

The dispersion curves of surface waves are displayed in figure 5 along with temperature variations for $T = 200$ K, $T = 220$ K, $T = 240$ K, $T = 260$ K, $T = 300$ K, $T = 320$ K, $T = 340$, $T = 360$, and $T = 380$. The hybrid curves at both the upper and lower frequency modes for Type-1 (i.e. 23.4 THz $< \omega <$ 24.9 THz) are predicted and occur with temperature variations. As temperature varies, the dispersion curve rises in contrast to the real part of the propagation constant (q). Figure 5(a) indicates that for the lower temperature range (i.e. $T = 200$ K), InSb behaves as a dielectric, so we have these curves due to phonon–phonon interaction. As hBN is dielectric polar in nature, it supports phonon interactions. The curves obtained in figure 5(b) show plasmon–polariton interaction akin to SPP modes because at high temperatures (i.e. $T > 200$ K), InSb shows its metallic nature [39, 41].

3.3.2. Effective mode index. The ratio of the propagation constant of the medium to the accessible space is known as the 'effective mode index N_{eff}.' Surface wave control is due to a normalized effective wave number such as $\mathrm{N_{eff}} = \frac{\mathrm{Re}\beta}{k_o}$. Figure 6 shows the temperatures ($T = 180$ K, 200 K, 220 K, 240 K, 340 K, 350 K, 360 K, and 380 K) whereby the SPP waves restricted on hBN-loaded InSb are shown at the lower frequency range of 23.9 THz. Figure 6(a) illustrates that the effective wave number of surface waves drops at lower temperatures, whereas it increases at higher temperatures. Therefore, such surface waves mediated by hBN-loaded TSMs increase with increasing temperature.

3.3.3. Phase velocity. A graphic representation of the effect of temperature on phase velocity can be found in figure 7.

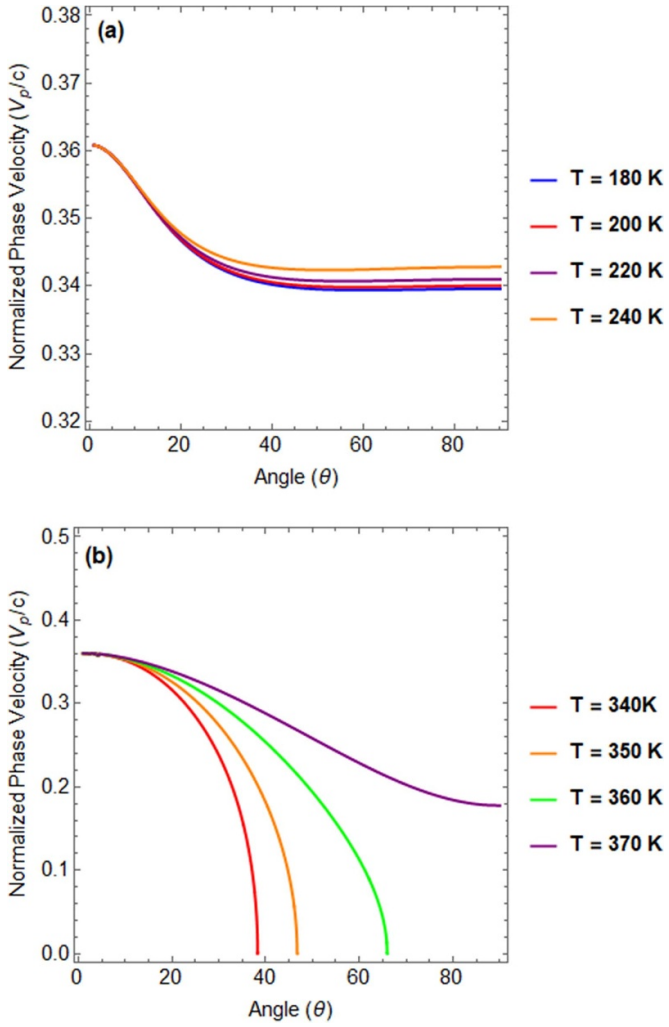

Figure 7. Thermal effects on phase velocity (V_P) against angle (θ) at 23.9 THz supported by hBN–InSb interface for Type-I surface wave propagation (a) $T \in [180,\ 240]$ K (b) $T \in [340,\ 370]$ K.

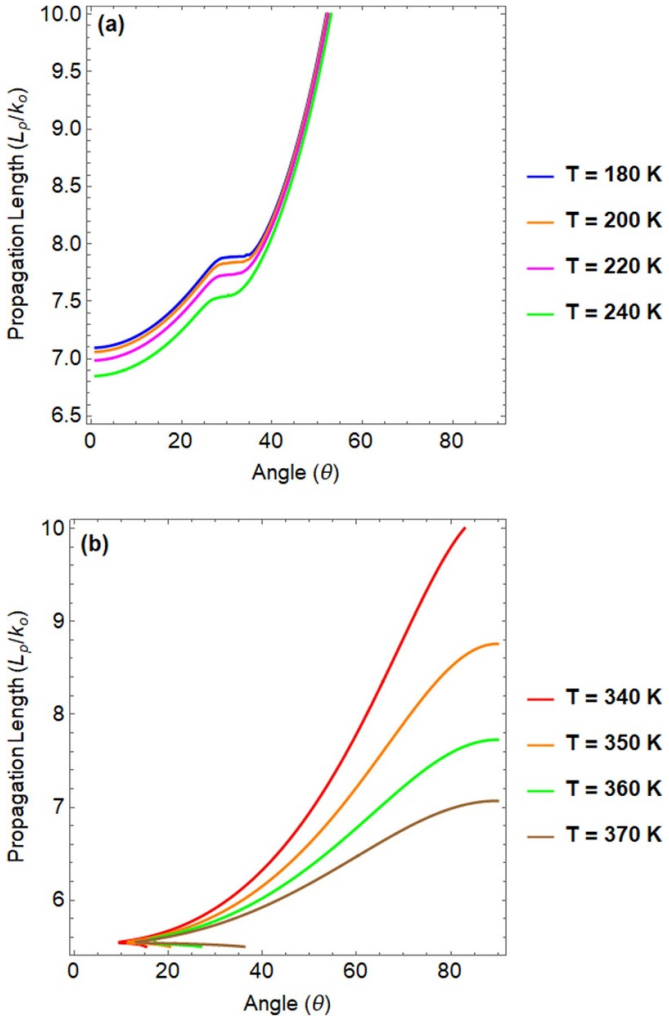

Figure 8. Propagation length (L_p) of surface waves versus angle (θ) under temperature variation at 23.9 THz supported by hBN–InSb interface for Type-I surface wave propagation (a) $T \in [180,\ 240]$ K (b) $T \in [300,\ 370]$ K.

The phase velocity is determined at the following temperatures: $T = 180$ K, 200 K, 220 K, 240 K, 340 K, 350 K, 360 K, and 370 K. Figure 7 clearly shows that the phase velocity is temperature dependent and that it may be adjusted. The normalized phase velocity increases at higher temperatures.

3.3.4. Propagation length. The imaginary part of the propagation constant is used to compute the propagation length (L_p), which is the length of time a surface wave stays at the interface between two mediums. Figure 8 illustrates how temperature affects the propagation length. Wave number k_o is used to normalize the propagation length. It illustrates how the propagation length decreases as temperature rises.

3.4. Surface waves at TSM–hyperbolic interface (Type- II)

Type-II hBN is linked to the upper RS band. The higher THz frequency range, or 41.1 THz $< \omega <$ 48.3 THz, is correlated with the higher RS band. The permittivity range for Type-II is $\varepsilon\| > 0$ and $\varepsilon\perp < 0$. The results of numerical computations are reported for Type-II based on characteristics like effective mode index, phase speed, and propagation distance.

3.4.1. Dispersion curve analysis. Figure 9 shows the temperature variations for $T = 180$ K, 200 K, 220 K, 240 K, 300 K, 340 K, 350 K, and 360 K in addition to the dispersion curves for Type-II. The much smaller temperature fluctuations

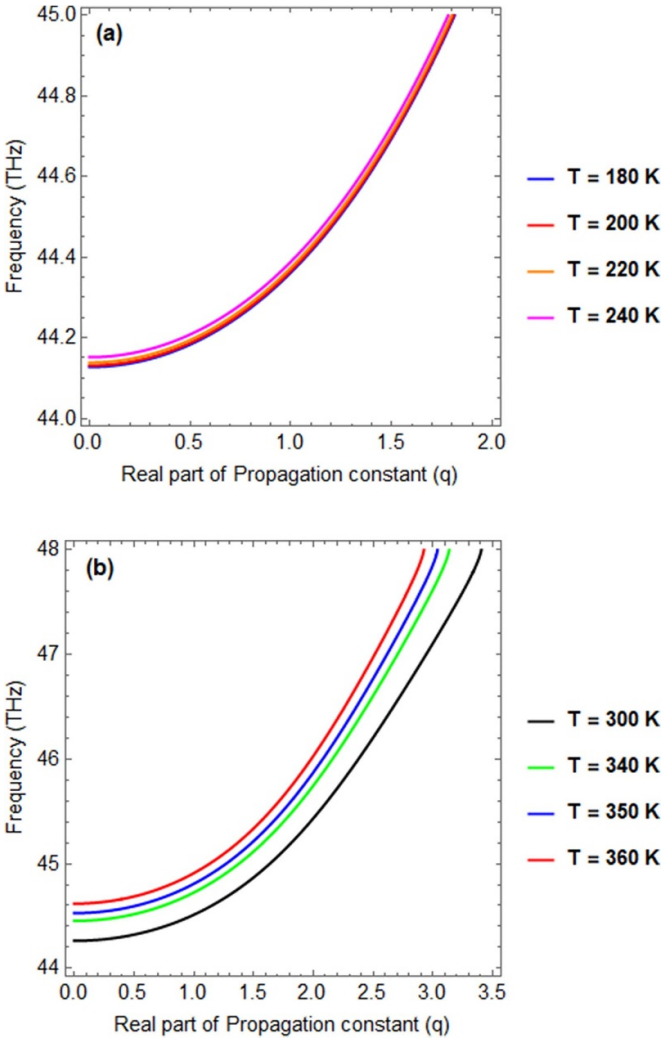

Figure 9. Dispersion curves for Type-II surface waves under temperature change supported by hBN–InSb interface. (a) $T \in [180,\ 240]$ K (b) $T \in [300,\ 360]$ K.

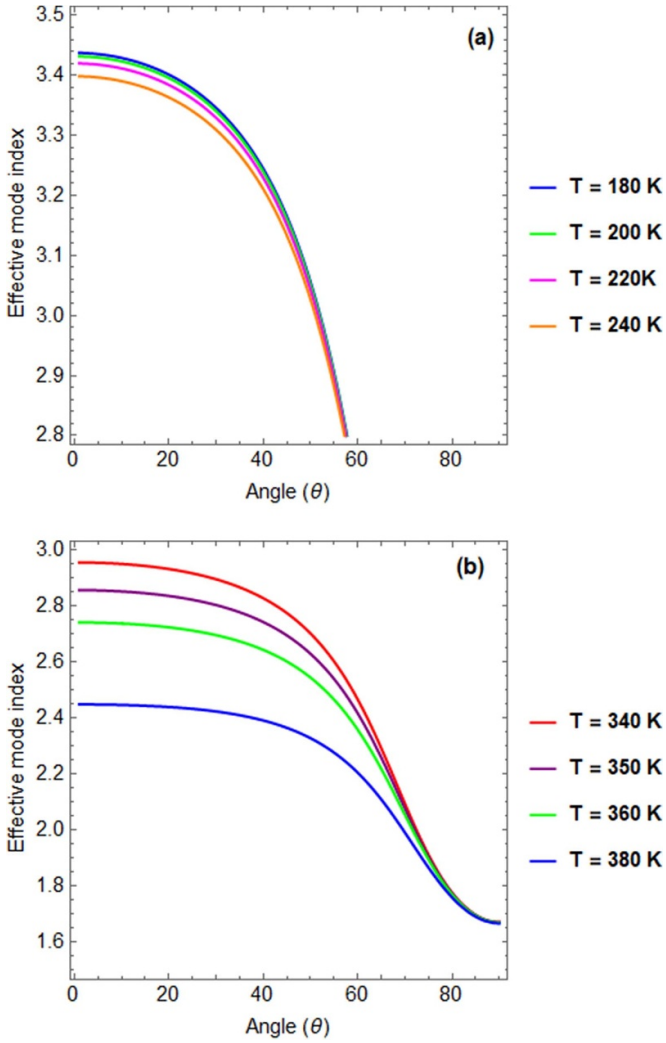

Figure 10. Impact of temperature on effective mode index 'Neff' for Type-II surface wave propagation assisted by hBN-InSb interface at 47.4 THz. (a) $T \in [180,\ 240]$ K (b) $T \in [340,\ 380]$ K.

are expected to result in dispersion curves at lower frequency modes for Type-II (i.e. 41.1 THz $< \omega <$ 48.3 THz). At higher temperatures, the dispersion curves show higher values.

3.4.2. Effective mode index. The influence of temperature on N_{eff} with respect to angle at the higher THz frequency range for Type-II is graphically demonstrated in figure 10 to aid in the further investigation of surface wave confinement. The contour plot method was used to compute a feasible solution. The figure shows that when the temperature rises, the effective surface wave number falls at the higher THz frequency range.

3.4.3. Phase velocity. Figure 11 provides a graphic depiction of how temperature affects phase velocity for Type-II. The phase velocity is determined at the following temperatures: $T = 180$ K, 200 K, 220 K, 240 K, 340 K, 350 K, 360 K, and 380 K. Thus, figure 11 indicates that phase velocity increases with temperature.

3.4.4. Propagation length. Figure 12 provides a graphic depiction of how temperature affects propagation length for Type-II. The phase velocity is determined at the following temperatures: $T = 180$ K, 200 K, 220 K, 240 K, 340 K, 350 K, 360 K, and 380 K. It is clear from figure 12 that propagation length decreases as temperature rises.

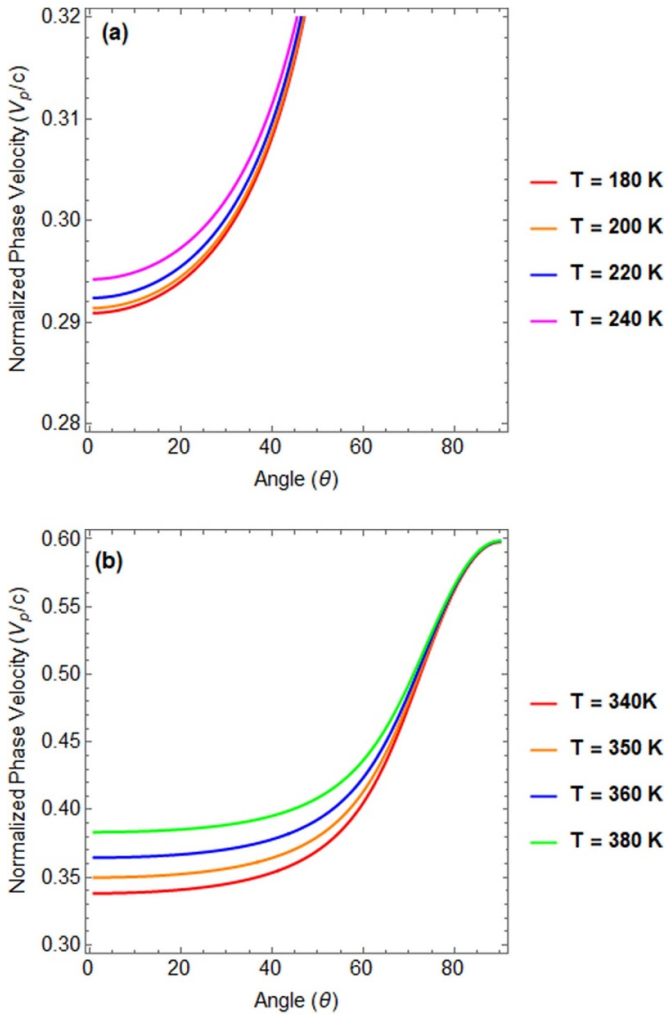

Figure 11. Influence of temperature on phase velocity (V_P) versus angle (θ) for Type-II surface wave propagation assisted by hBN-InSb interface at 47.4 THz. (a) $T \in [180,\ 240]$ K (b) $T \in [340,\ 380]$ K.

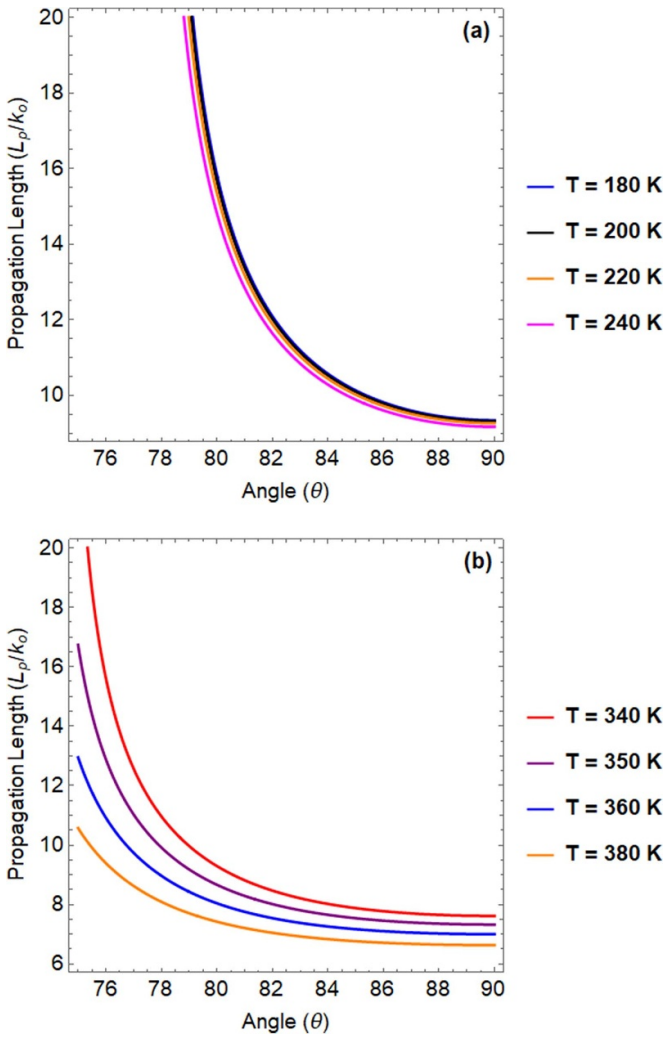

Figure 12. Propagation length L_p versus angle (θ) for Type-II surface wave propagation assisted by hBN-InSb interface at 47.4 THz. (a) $T \in [180,\ 240]$ K (b) $T \in [340,\ 380]$ K.

4. Concluding remarks

This study mainly concentrated on the thermally tunable EMS waves originating from hBN-loaded InSb. It demonstrated that the propagation features associated with surface waves (propagation length profile, phase velocity, effective mode index, and dispersion curve) are temperature dependent. The following conclusions were drawn as a result of the numerical results: SPP waves are similar to EMS waves generated by the interface of InSb loaded with hBN. As an external variable, temperature actively controls the parameters of surface wave propagation, including phase speed, propagation length, surface wave confinement, and dispersion relation. It can be concluded that for the type-I i.e. surface waves at TSM–elliptic interface, for lower temperature range, the hBN-InSb interface supports phonon–phonon interactions while for the high temperature range, plasmon–polariton interaction akin to SPP modes are dominated. For the type-II i.e. surface waves at TSM–hyperbolic interface support the bulk modes and the temperature plays a vital role in the tuning the resonance frequency of the modes. Further, the excitation frequency tunability provides additional flexibility to modify the surface wave propagation parameters for Type-I and Type-II. The computed numerical outcomes of this study may be beneficial for the development of thermo-optical sensor designs, near-field thermal imaging, THz photoemission temperature-assisted communication systems, and spectroscopy platforms.

Data availability statement

All data that support the findings of this study are included within the article (and any supplementary files).

Acknowledgment

This work was supported by the Researchers Supporting Project Number (RSPD2024R985), King Saud University, Riyadh, Saudi Arabia.

Authors' Contributions

Tahseen Sana and Muhammad Zeshan Yaqoob wrote main manuscript and derived analytical expressions. Majeed A S Alkanhal and Abdul Ghaffar edited the manuscript and reviewed the numerical analysis., Ahtisham Ali, Hafeez Ullah and Yasin developed methodology and conducted the analysis of results and discussion in the given study. All authors reviewed the manuscript before submission.

ORCID iDs

Tahseen Sana https://orcid.org/0009-0000-1014-8904
Majeed A S Alkanhal https://orcid.org/0000-0003-3673-0411
Ahtisham Ali https://orcid.org/0009-0008-8052-1346
Hafeez Ullah https://orcid.org/0000-0003-0640-2628
Muhammad Zeshan Yaqoob https://orcid.org/0000-0001-9145-8604

References

[1] Gupta S and Caloz C 2017 Real-time electromagnetic signal processing: principles and illustrations *Wave Propagation Concepts for Near-Future Telecommunication Systems* (IntechOpen) (https://doi.org/10.5772/67356)
[2] Nikolaev A *et al* 2021 Surface electromagnetic wave-based wireless communication system for mines *IOP Conf. Ser.: Earth Environ. Sci.* **720** 012032
[3] Roy S, Misra A and Abdikian A 2023 Modulation of electromagnetic waves in a relativistic degenerate plasma at finite temperature *Phys. Fluids* **35** 066123
[4] Yoo M, Kim H K and Lim S 2016 Electromagnetic-based ethanol chemical sensor using metamaterial absorber *Sens. Actuators* B **222** 173–80
[5] Nzao A B S 2021 Study and modeling of human biological tissue exposed to high frequency electromagnetic waves *Open J. Appl. Sci.* **11** 1109–21
[6] Ali A, El-Mellouhi F, Mitra A and Aïssa B 2022 Research progress of plasmonic nanostructure-enhanced photovoltaic solar cells *Nanomaterials* **12** 788
[7] Stedwell C N and Polfer N C 2013 Spectroscopy and the electromagnetic spectrum *Laser Photodissociation and Spectroscopy of Mass-separated Biomolecular Ions* (Springer) pp 1–20
[8] Janani A S, Darvazehban A, Rezaeieh S A and Abbosh A M 2022 Focused planar electromagnetic waves for enhanced near-field microwave imaging with verification using tapered gradient-index lens antenna *IEEE Access* **10** 86920–34
[9] Ding S-Y, You E-M, Tian Z-Q and Moskovits M 2017 Electromagnetic theories of surface-enhanced Raman spectroscopy *Chem. Soc. Rev.* **46** 4042–76
[10] Tabatabaeian Z S 2023 Highly Q-factor THz sensor for biosensing based on traveling wave propagation in the metamaterial cavity *Optik* **287** 171098
[11] Jin Z 2023 Analysis of electromagnetic wave applications and development *Highlights Sci. Eng. Technol.* **68** 172–81
[12] Schultz D A 2003 Plasmon resonant particles for biological detection *Curr. Opin. Biotechnol.* **14** 13–22
[13] Specht M, Pedarnig J D, Heckl W M and Hänsch T W 1992 Scanning plasmon near-field microscope *Phys. Rev. Lett.* **68** 476
[14] Qiu C *et al* 2019 Design and analysis of a novel graphene-assisted silica/polymer hybrid waveguide with thermal–optical phase modulation structure *IEEE Photon. J.* **11** 1–10
[15] Polo J, Mackay T and Lakhtakia A 2013 *Electromagnetic Surface Waves: A Modern Perspective* (Newnes)
[16] D'yakonov M I 1988 New type of electromagnetic wave propagating at an interface *Sov. Phys-JETP* **67** 714–6 (available at: www.jetp.ras.ru/cgi-bin/e/index/e/67/4/p714?a=list)
[17] Takayama O, Artigas D and Torner L 2014 Lossless directional guiding of light in dielectric nanosheets using Dyakonov surface waves *Nat. Nanotechnol.* **9** 419–24
[18] Zapata-Rodríguez C J, Miret J J, Vuković S and Belić M R 2013 Engineered surface waves in hyperbolic metamaterials *Opt. Express* **21** 19113–27
[19] Walker D, Glytsis E and Gaylord T 1998 Surface mode at isotropic–uniaxial and isotropic–biaxial interfaces *J. Opt. Soc. Am.* A **15** 248–60
[20] Gao J, Lakhtakia A and Lei M 2010 Dyakonov-Tamm waves guided by the interface between two structurally chiral materials that differ only in handedness *Phys. Rev.* A **81** 013801
[21] Crasovan L-C, Artigas D, Mihalache D and Torner L 2005 Optical Dyakonov surface waves at magnetic interfaces *Opt. Lett.* **30** 3075–7
[22] Pulsifer D P, Faryad M and Lakhtakia A 2013 Observation of the Dyakonov-Tamm wave *Phys. Rev. Lett.* **111** 243902
[23] Ghodrati M, Mir A and Wen J 2024 Metamaterials and metasurfaces for sensor and biosensor applications *Electromagnetic Wave Control Techniques of Metasurfaces and Metamaterials* (IGI Global) pp 61–105
[24] Moon S, Kim J, Park J, Im S, Kim J, Hwang I and Kim J K 2023 Hexagonal boron nitride for next-generation photonics and electronics *Adv. Mater.* **35** 2204161
[25] Dai S *et al* 2014 Tunable phonon polaritons in atomically thin van der Waals crystals of boron nitride *Science* **343** 1125–9
[26] Hajian H, Rukhlenko I D, Hanson G W, Low T, Butun B and Ozbay E 2020 Tunable plasmon-phonon polaritons in anisotropic 2D materials on hexagonal boron nitride *Nanophotonics* **9** 3909–20
[27] Merano M 2016 Transverse electric surface mode in atomically thin Boron–Nitride *Opt. Lett.* **41** 2668–71
[28] Zhu B, Ren G, Gao Y, Wang Q, Wan C, Wang J and Jian S 2016 Dyakonov surface waves at the interface between hexagonal-boron-nitride and isotropic material *J. Opt.* **18** 125006
[29] Wang J, Ma F and Sun M J R A 2017 Graphene, hexagonal boron nitride, and their heterostructures: properties and applications *RSC Adv.* **7** 16801–22
[30] Cheng M, Fu P and Chen S J O C 2021 Tunable Dyakonov surface waves in graphene-hBN hyperstructure *Opt. Commun.* **482** 126630
[31] Laturia A *et al* 2018 Dielectric properties of hexagonal boron nitride and transition metal dichalcogenides: from monolayer to bulk *npj 2D Mater. Appl.* **2** 6
[32] Aharonovich I, Tetienne J-P and Toth M 2022 Quantum emitters in hexagonal boron nitride *Nano Lett.* **22** 9227–35
[33] Wang Y, Lee J, Zheng X-Q, Xie Y and Feng P X-L 2019 Hexagonal boron nitride phononic crystal waveguides *ACS Photonics* **6** 3225–32
[34] Dai S *et al* 2018 Manipulation and steering of hyperbolic surface polaritons in hexagonal boron nitride *Adv. Mater.* **30** 1706358
[35] Ogawa S, Fukushima S and Shimatani M 2023 Hexagonal boron nitride for photonic device applications: a review *Materials* **16** 2005

[36] Vassalini I, Alessandri I and de Ceglia D 2021 Stimuli-responsive phase change materials: optical and optoelectronic applications *Materials* **14** 3396
[37] Zhang C, Liu Y, Li J, Wu Q and Li M 2024 Design of a highly sensitive terahertz temperature and refractive index composite sensor based on an InSb–Ag composite grating *J. Opt. Soc. Am.* B **41** 411–20
[38] Mackay T G and Lakhtakia A 2019 Surface waves with negative phase velocity supported by temperature-dependent hyperbolic materials *J. Opt.* **21** 085103
[39] Moradi M 2023 Thermally tunable Dyakonov surface waves in semiconductor nanowire metamaterials *Sci. Rep.* **13** 12353
[40] Yaqoob M, Ahamd M, Ghaffar A, Razzaz F, Saeed S M and Alanazi T M 2023 Thermally tunable electromagnetic surface waves supported by graphene loaded indium antimonide (InSb) interface *Sci. Rep.* **13** 18631
[41] Sana T, Alkanhal M A S, Ali A, Ullah H, Ghaffar A, Khan Y and Yaqoob M Z 2024 Hybrid Dyakonov surface waves at uniaxial crystal-temperature-sensitive material interfaces *Int. J. Opt.* **2024** 5757834
[42] Rahou D, Bekhouche H, Ghezal E A, Gueddim A, Bouarissa N and Ziani H 2020 Electronic and optical properties of InSb quantum dots from pseudopotential calculation *Chin. J. Phys.* **66** 206–13
[43] Yang D *et al* 2024 Methods for preparation of hexagonal boron nitride nanomaterials *Chem. Mater.* (https://doi.org/10.1021/acs.chemmater.4c00582)
[44] Shi N, Li L, Gao P, Jiang X, Hao J, Ban C, Zhang R and Liu Z 2022 Synthesis of two-dimensional hexagonal boron nitride and mid-infrared nanophotonics *ACS Appl. Electron. Mater.* **5** 34–65